Available online at www.sciencedirect.com
SCIENCE DIRECT®
ELSEVIER
International Journal of Solids and Structures 42 (2005) 3591–3609
INTERNATIONAL JOURNAL OF SOLIDS and STRUCTURES
www.elsevier.com/locate/ijsolstr

Sensitivity analysis for fixed-grid shape optimization by using oblique boundary curve approximation

Gang-Won Jang [a], Yoon Young Kim [b,*]

[a] School of Mechanical Engineering, Kunsan National University, Kunsan, Chonbuk 573-701, Republic of Korea
[b] School of Mechanical and Aerospace Engineering, National Creative Research Initiatives Center for Multiscale Design, Seoul National University, Shinlim-Dong San 56-1, Seoul 151-742, Republic of Korea

Received 30 October 2003
Available online 10 December 2004

Abstract

The remesh-free property is the most attractive feature of the various versions of fixed-grid-based shape optimization methods. When the design boundary curves do not pass through the predetermined analysis grids, however, the element stiffness as well as the stress along the curves may be computed inaccurately. Even with the popular area-fraction-based stiffness evaluation approach, the whole optimization process may become quite inefficient in such a case. As an efficient alternative approach, we considered a stiffness matrix evaluation method based on the boundary curve approximation by piecewise oblique curves which can cross several elements. The main contribution of this work is the analytic derivation of the shape sensitivity for the discretized system by the fixed-grid method. Since the force term in the sensitivity equation is associated only with the elements crossed by the design boundary curve, we only need the design velocities of the intersecting points between the curve and the fixed mesh. The present results obtained for two-dimensional elasticity and Poisson's problems are valid for both the single-scale standard fixed-grid method and the multiscale fictitious domain-based interpolation wavelet-Galerkin method.

Keywords: Sensitivity analysis; Shape optimization; Fixed-grid method; Fictitious domain method; Wavelet-Galerkin method

1. Introduction

In the standard shape optimization based on the finite element approach, remeshing cannot be avoided during the optimization process if accurate analysis is to be guaranteed, especially for design problems

* Corresponding author. Tel.: +82 28807154; fax: +82 28831513.
E-mail address: yykim@snu.ac.kr (Y.Y. Kim).

0020-7683/$ - see front matter © 2004 Elsevier Ltd. All rights reserved.
doi:10.1016/j.ijsolstr.2004.10.029

requiring large shape changes (Bennett and Botkin, 1985; Yao and Choi, 1989). Researchers have shown recent interest on the shape optimization based on the fixed-grid analysis or the Eulerian-type analysis because the analysis offers way to avoid cumbersome remeshing processes. Another advantage of the fixed-grid-based shape optimization method is that it requires only the boundary velocity field for design updates while the standard finite-element-based shape optimization method generally requires design velocities for all nodes, the so-called domain and boundary velocity fields (Choi and Chang, 1994). The fixed-grid based method shows this feature because its analysis nodes are independent of the shape changes.

Though the fixed-grid method is equipped with the excellent remesh-free property, this method has some difficulties in accurately evaluating the stiffness matrices of the elements adjacent to curved boundaries. It has this difficulty mainly because the analysis grids or nodes are always predetermined, and the design boundary does not necessarily pass through these analysis grid points. Since the present sensitivity analysis is mainly for a method to overcome such a difficulty, it is worth stating the implementation technique of the fixed-grid method for shape optimization.

In implementing the remesh-free fixed-grid analysis method, the most popular approach is to embed the original design domain ω encircled by curved boundaries into a fictitious domain Ω usually having a simple geometry. Then, the fixed-grid-based analysis is carried out for Ω. In Fig. 1, we illustrate a rectangular fictitious domain for a generally-shaped ω. The single-scale fixed-grid method usually uses uniformly distributed rectangular finite elements for two-dimensional cases. The stiffness of the elements inside ω is set to be the stiffness of the original material, but the elements inside $\Omega\backslash\omega$ are assigned to have a very weak material. The question is: How does one evaluate the stiffness of the boundary elements lying on the boundary $\partial\omega$. In the fixed-grid method, the stiffness of the boundary elements changes when the boundary curve changes. Therefore, the boundary element stiffness must be estimated accurately for efficient shape optimization.

Until recently, the common approach has been the area-fraction-based stiffness evaluation method, as was used in Garcia and Steven (1998) and Kim and Chang (2003, submitted for publication). The concept of this approach is to evaluate the boundary element stiffness proportionally to the area fraction of the part belonging to ω within the boundary element. The boundary design velocity is thus related to the rate of the change of the area fraction of the boundary element. However, the boundary curve in this method needs to be approximated by zigzags that consist only of vertical and horizontal lines, so this area-fraction-based approach is not effective for curved boundaries. The only way to obtain accurate solutions near the boundary is to work with highly-dense grid distributions.

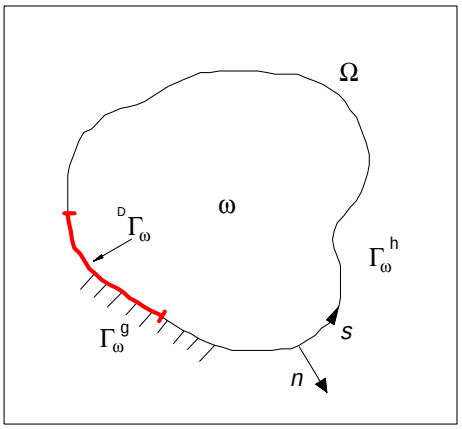

Fig. 1. A two-dimensional problem with the domain of interest ω embedded in a fictitious domain Ω (Γ_{ω}^{g}: boundary under kinematic constraint, Γ_{ω}^{h}: boundary under natural condition, $^{D}\Gamma_{\omega}$: design boundary).

In order to obtain accurate solutions near the curved boundary without excessive grid densities, Jang et al. (2002, 2003) proposed a more direct approach; a curved boundary is approximated by piecewise oblique lines formed by the connections of the points between the curved boundary and the fixed-grid lines. In this case, the piecewise oblique line, the approximated boundary curve, does not usually pass through the analysis nodes. Therefore, the stiffness matrix of a boundary element should be integrated separately by considering the oblique line on the element, but this integration can be easily performed by the Gauss quadrature. Jang et al. (2002, 2003) used this idea for the shape optimization method based on the adaptive multiscale interpolation wavelet-Galerkin method; the standard fixed-grid method is a non-adaptive, single-scale version of the wavelet-Galerkin method. Thus the piecewise oblique boundary curve approximation scheme works equally for the standard fixed-grid method. In Jang et al. (2002, 2003), however, the resulting sensitivity analysis was carried out by the direct finite difference scheme.

In this work, we present the semi-analytic sensitivity analysis for the fixed-grid shape optimization based on the oblique boundary curve approximation. By the semi-analytic analysis, we mean the analytic sensitivity analysis for a discretized structural system, or the continuum-discrete sensitivity analysis (Choi and Kim, in press). In the first part of this work, some results derived by Hansen et al. (2001) are utilized for the present analysis; the analysis grids not interacting with the boundary curves are stationary or fixed during the whole design process both in the method by Hansen et al. (2001) and in the oblique boundary curve approximation method. The sensitivity equations and the boundary conditions are derived for two-dimensional Poisson problems and elasticity problems. The shape change will be represented by the movement of the intersection points. The force vector for the sensitivity equations comes only from the boundary velocity fields of the intersection points. Once the semi-analytic sensitivity is calculated, it may be used to check the accuracy of the sensitivity by the finite difference scheme. To this end, we considered a domain having a simple geometry parameterized by a Bezier curve and compared the numerical and analytical sensitivities. The shape sensitivity for a microgripper whose boundary is parameterized by a B-spline curve was also considered for verification. Finally, we also remark on how the present sensitivity analysis based on the single-scale fixed-grid method can be extended for the multiscale interpolation wavelet-Galerkin method.

2. Various boundary curve approximations for fixed-grid shape optimization

In Fig. 2, we illustrate several boundary approximation techniques based on fixed-grid or fixed-basis functions. The vertical axis of the ellipse in Fig. 2(a) is considered as the design parameter and the design changes to the lower figure in Fig. 2(a).

Fig. 2(b) shows the approximated geometry of the ellipse using the area-fraction-based approximation. The ellipse is embedded into a rectangular fictitious domain, which is divided into elements with fixed mesh. In the figure, the gray level of the elements represents the area fraction which is defined as

$$\alpha^{\mathrm{e}} = \frac{A^{\mathrm{e}}_{\omega}}{A^{\mathrm{e}}} \tag{1}$$

where A^{e} and A^{e}_{ω} stand for the area of the element and the portion of A^{e} lying inside the domain of interest ω, respectively. For elements inside ω, $\alpha^{\mathrm{e}} = 1$ and $\alpha^{\mathrm{e}} = 0$ for elements outside ω.

Using the area fraction in Eq. (1), the material property $\mathbf{C}^{\mathrm{e}}$ for a boundary element is approximated as

$$\mathbf{C}^{\mathrm{e}} = \alpha^{\mathrm{e}}\mathbf{C} + (1-\alpha^{\mathrm{e}})\gamma\mathbf{C}, \quad 0 < \gamma \ll 1 \tag{2}$$

where $\mathbf{C}^{\mathrm{e}}$ is the material property of the element inside ω.

Thus, the design change in the area-fraction-based approximation method is represented by the change of the material property of boundary elements. The design sensitivity can be, therefore, expressed with the sensitivity of the area fraction:

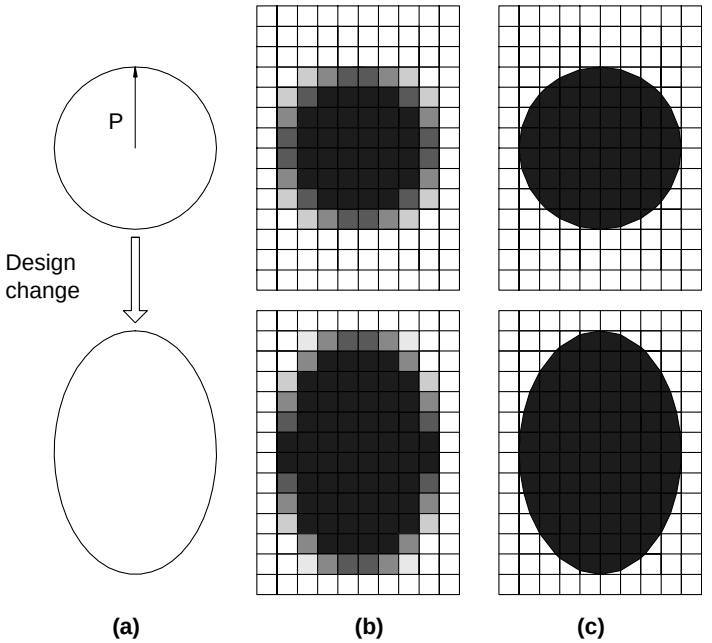

Fig. 2. Boundary approximation techniques for (a) the design change of an ellipse, (b) the area-fraction-based approximation and (c) the present approximation using oblique boundary lines.

$$\frac{\mathrm{d}\alpha^{\mathrm{e}}}{\mathrm{d}z} = \frac{1}{A^{\mathrm{e}}}\frac{\mathrm{d}}{\mathrm{d}z}\int\int_{\omega^{\mathrm{e}}} \mathrm{d}\omega = \frac{1}{A^{\mathrm{e}}}\int_{\partial\omega^{\mathrm{e}}} \mathbf{V}\cdot\mathbf{n}\,\mathrm{d}\Gamma \tag{3}$$

where z is the design parameter, ω^{e} is the ω-inside region of the boundary element and $\mathbf{V}$ means the boundary design velocity with respect to z. The unit vector outward normal to the boundary is expressed as $\mathbf{n}$. In Eq. (3), we use the following formula (see Haug et al., 1986 for the proof):

$$\frac{\mathrm{d}}{\mathrm{d}z}\int\int_{\omega} f\,\mathrm{d}\omega = \int\int_{\omega}\frac{\partial f}{\partial z}\,\mathrm{d}\omega + \int_{\partial\omega} f\mathbf{V}\cdot\mathbf{n}\,\mathrm{d}\Gamma \tag{4}$$

Using Eq. (3), Kim and Chang (2003, submitted for publication) derived the design sensitivity for the area-fraction-based approximation method and applied it to a torque arm design problem undergoing a relatively large shape change.

When local performance measures such as heat fluxes or stresses are used as design constraints in shape optimization, local measures must be evaluated accurately to speed up the optimization process and improve the quality of the final design. Since most local design constraints are measured on the design boundary, the quality of boundary approximation plays a key role in shape optimization based on the fixed-grid method. The zigzag approximation of the area-fraction-based approximation method yields, however, inaccurate values near the domain boundary. As a result, extremely many elements are required to recover the accuracy, which leads to high numerical cost.

To deal with such accuracy problem on the domain boundary, Jang et al. (2003) directly approximated the boundary with piecewise oblique lines. As illustrated in Fig. 2(c), their approach significantly improved the quality of the approximated boundary. The intersection points between the original boundary $\partial\omega$ and boundary elements are determined first, and then simply connected to construct the oblique boundary lines $\Gamma_{\omega}^{\mathrm{e}}$ as in Fig. 3. The oblique boundary usually crosses the boundary element domain without passing

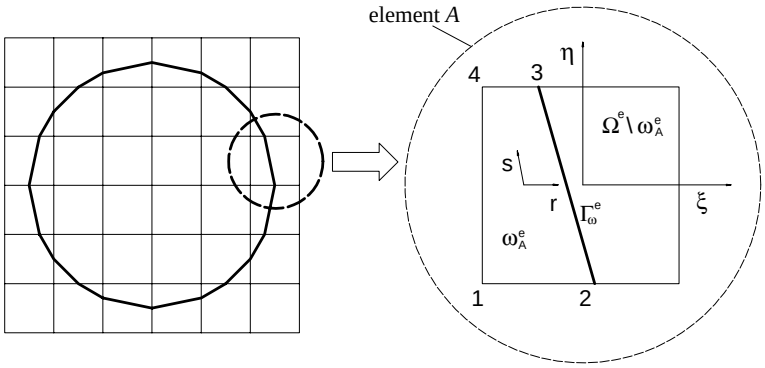

Fig. 3. A circular boundary approximated by piecewise oblique lines.

through the analysis nodes. For the sensitivity analysis, the parametric values of the intersection points as well as their locations should be calculated because they are required to calculate the boundary velocities.

Consider now the calculation of the stiffness matrix $\mathbf{k}^e$ of the boundary element in Fig. 3. For plane elasticity problems, the element stiffness matrix $\mathbf{k}^e$ is given as

$$\mathbf{k}^e = \int_{-1}^{1}\int_{-1}^{1} \mathbf{B}^T(\xi,\eta)\mathbf{C}^e(\xi,\eta)\mathbf{B}(\xi,\eta)|\mathbf{J}|\,d\xi\,d\eta \tag{5}$$

where $\mathbf{B}$ is the matrix relating strains to nodal displacements, $\mathbf{C}^e$ is the matrix with the elasticity coefficients. The Jacobian $|\mathbf{J}|$ is simply one quarter of the element area in this case. On the boundary elements, $\mathbf{C}^e$ is not uniform:

$$\mathbf{C}^e = \begin{cases} \mathbf{C} & \text{in } \omega_A^e \\ \varepsilon\mathbf{C} & \text{in } \Omega^e \setminus \omega_A^e \end{cases} \tag{6}$$

where ε is a small positive number.

The integration of Eq. (5) is, therefore, performed separately for ω_A^e and $\Omega^e \setminus \omega_A^e$. To this end, we introduce another coordinates (r,s) in addition to the element local coordinates (ξ,η). The coordinates of (r,s) map a normalized rectangular domain $[-1,1]\times[-1,1]$ to ω_A^e, i.e., the region bounded by 1–2–3–4 in Fig. 3. The relation between (ξ,η) and (r,s) can be given as

$$\begin{pmatrix}\xi\\ \eta\end{pmatrix} = \sum_{i=1}^{4} N_i(r,s)\begin{pmatrix}\xi_i\\ \eta_i\end{pmatrix} \tag{7}$$

where (ξ_i,η_i) are the local coordinates of points 1, 2, 3 and 4 in Fig. 3 and $N_i(r,s)$ represent standard bilinear functions. If ω_A^e becomes a triangular region, it can be also treated by (7) as a degenerate case.

Using Eq. (7), the element stiffness in (5) can be written as

$$\begin{aligned}\mathbf{k}^e &= \varepsilon\int_{-1}^{1}\int_{-1}^{1} \mathbf{B}^T(\xi,\eta)\mathbf{C}\mathbf{B}(\xi,\eta)|\mathbf{J}|\,d\xi\,d\eta + (1-\varepsilon)\int\int_{\omega_A^e} \mathbf{B}^T(\xi,\eta)\mathbf{C}\mathbf{B}(\xi,\eta)|\mathbf{J}|\,d\xi\,d\eta \\ &= \varepsilon\int_{-1}^{1}\int_{-1}^{1} \mathbf{B}^T(\xi,\eta)\mathbf{C}\mathbf{B}(\xi,\eta)|\mathbf{J}|\,d\xi\,d\eta \\ &\quad + (1-\varepsilon)\int_{-1}^{1}\int_{-1}^{1} \mathbf{B}^T(\xi(r,s),\eta(r,s))\mathbf{C}\mathbf{B}(\xi(r,s),\eta(r,s))|\mathbf{J}||\hat{\mathbf{J}}|\,dr\,ds\end{aligned} \tag{8}$$

where $\hat{\mathbf{J}}$ is the Jacobian relating (r,s) and (ξ,η).

In case $\Omega^e \setminus \omega_A^e$ is a triangle, (r,s) maps a normalized rectangle to $\Omega^e \setminus \omega_A^e$ and $\mathbf{k}^e$ becomes

$$\mathbf{k}^e = \int_{-1}^{1}\int_{-1}^{1} \mathbf{B}^T(\xi,\eta)\mathbf{C}\mathbf{B}(\xi,\eta)|\mathbf{J}|\,d\xi\,d\eta - (1-\varepsilon)\int_{-1}^{1}\int_{-1}^{1} \mathbf{B}^T(\xi(r,s),\eta(r,s))\mathbf{C}\mathbf{B}(\xi(r,s),\eta(r,s))|\mathbf{J}||\hat{\mathbf{J}}|\,dr\,ds \tag{9}$$

The stiffness matrix evaluation in Eqs. (8) or (9) is applied only to the boundary elements. It only requires small additional expenses to calculate the intersection points and element stiffness matrices along the boundary of the domain. Therefore, the main advantages of the area-fraction-based approximation method such as fast meshing and efficient stiffness matrix formulation are still preserved.

To calculate the element force vector, the following formula will be used:

$$\mathbf{f}^e = \int_{-1}^{1}\int_{-1}^{1} \mathbf{N}(\xi,\eta)^T\mathbf{f}|\mathbf{J}|\,d\xi\,d\eta$$

where $\mathbf{f}$ is the applied force and $\mathbf{N}$ is the matrix representing the bilinear shape functions. If $\mathbf{f}$ is a boundary force such as pressure, the above equation is rewritten as

$$\mathbf{f}^e = \int_{\Gamma_\omega^e} \mathbf{N}^T\mathbf{f}\,d\varsigma$$

where ς is the coordinate on the oblique boundary Γ_ω^e. The strict imposition of the Dirichlet condition or the kinematic constraint is difficult for the fixed-grid-type methods as long as the boundary under constraint does not pass through the fixed grids. In this case, the kinematic constraint of the boundary is prescribed on the grids nearest to the constrained boundary.

3. Sensitivity analysis for the oblique boundary curve approximation

Hansen et al. (2001) derived a sensitivity equation and its boundary conditions for the fixed-basis finite element method. They showed that, in a stationary coordinate system, the stiffness matrix for the sensitivity problem is the same as that of the reference problem, and the force vector for the sensitivity problem arises only from the boundary elements of a design boundary. The fictitious domain method is not employed in their research, and the area for a boundary element extends or shrinks with its nodes fixed as the design changes. So, the normalized area for the boundary element is no more $[-1,1]^2$. It may be difficult to have consistent fixed mesh throughout the whole optimization process. New sets of fixed-basis finite elements should be introduced to avoid extreme aspect ratios of boundary elements after updating the shape.

In this work, we derived the sensitivity equation and its boundary conditions for the fixed-grid method with oblique boundary curve approximation by using some results given by Hansen et al. (2001). First, we began with the sensitivity analysis of a one-dimensional problem with fixed-basis functions using the fictitious domain. Though the fictitious domain method is impractical for one-dimensional problems, we used the approach for the general derivation of sensitivity for problems of higher dimensions. The induced equations are extended to two-dimensional Poisson equations and elasticity problems.

3.1. Overview on the fixed-grid sensitivity analysis with a one-dimensional example

In the shape optimization with the standard finite element analysis, the sensitivity of a solution is generally given as

$$\frac{\mathrm{d}u(\mathbf{x};z)}{\mathrm{d}z}=\frac{\partial u}{\partial z}+\sum_{i=1}^{N}\frac{\partial u}{\partial x_i}\frac{\partial x_i}{\partial z}=\bar{u}+\sum_{i=1}^{N}\frac{\partial u}{\partial x_i}V_i \tag{10}$$

where $u(\mathbf{x};z)$ denotes a solution of an N-dimensional problem. The symbol $\dot{(\cdot)}$ denotes the partial derivative $\partial(\cdot)/\partial z$ while $\mathrm{d}(\cdot)/\mathrm{d}z$ represents the material derivative. The coordinates x_i in Eq. (10) are the convected coordinates which change as the design changes. The symbol V_i in Eq. (10) denotes the change rate of the coordinates with respect to the design change and referred to as the design velocity. The field of V_i does not need to be unique as long as it satisfies the conditions of regularity and linear dependency (Choi and Chang, 1994). However, when the fixed grids are used in the analysis, the coordinates are stationary and independent of the design change, so the sensitivity of a solution can be simply written as

$$\frac{\mathrm{d}u(\mathbf{x};z)}{\mathrm{d}z}=\bar{u} \tag{11}$$

To derive the equation for the sensitivity $\bar{u}$, we begin with a one-dimensional problem:

$$-(ku')'=f \tag{12a}$$

$$u=0 \quad \text{at } x=0 \tag{12b}$$

$$u'=0 \quad \text{at } x=z \tag{12c}$$

where the domain of interest $\omega=[0,z]$ and the right end of the domain is set as the design parameter. In Eq. (12a), $(\cdot)'$ denotes the one-dimensional spatial derivative. In Fig. 4, the domain ω is illustrated with its embracing fictitious domain Ω and weak material property, εk , is imposed on $\Omega\backslash\omega$.

The total potential energy of the problem in Eq. (12) can be written as

$$\Phi(u(x;z);z)=\int_{x=0}^{z}\left\{\frac{1}{2}k(u'(x;z))^2-fu(x;z)\right\}\mathrm{d}x+\int_{x=z}^{L}\frac{1}{2}\varepsilon k(u'(x;z))^2\,\mathrm{d}x \tag{13}$$

with the kinematic constraint

$$u=0 \quad \text{at } x=0 \tag{14}$$

Note that $u'=0$ is assumed at $x=L$ in Eq. (13).

The kinematically admissible u minimizing Eq. (13) is the solution of Eqs. (12). When the change of the domain ω is smooth enough to guarantee the smooth change of the solution, the solution for the problem with a perturbed design minimizes the perturbed total potential. So, the solution for the perturbed problem satisfies

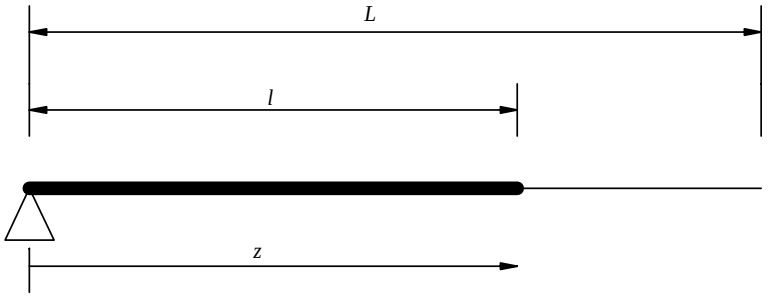

Fig. 4. One-dimensional problem with the domain of interest $\omega=[0,l]$ embedded in a fictitious domain $\Omega=[0,L]$.

$$\delta_u \Phi(u(x; z+\Delta z); z+\Delta z) = 0 \tag{15}$$

with the same boundary condition as in Eq. (14).

A Taylor's expansion of Eq. (15) about a reference domain $[0, z]$ is

$$\delta_u \Phi(u(x; z+\Delta z); z+\Delta z) = \delta_u \Phi(u(x; z); z) + \delta_u \bar{\Phi}(u(x; z); z)\Delta z + \tfrac{1}{2}\delta_u \bar{\bar{\Phi}}(u(x; z); z)\Delta z^2 + \cdots = 0 \tag{16}$$

Because Eq. (16) holds for varying Δz, it leads to

$$\delta_u \Phi(u(x; z); z) = 0 \tag{17a}$$

$$\delta_u \bar{\Phi}(u(x; z); z) = 0 \tag{17b}$$

$$\delta_u \bar{\bar{\Phi}}(u(x; z); z) = 0, \ \ldots \tag{17c}$$

Eq. (17a) gives the solution $u(x; z)$ for the reference problem. The sensitivity problem in Eq. (17b) yields the solution sensitivity $\bar{u}(x; z)$ and the higher order terms in (17c) are not considered in this research.

The variation of the total potential in Eq. (13) is given as

$$\delta_u \Phi(u(x; z); z) = \int_{x=0}^{z} \{k u'(x; z)\delta u'(x; z) - f\delta u(x; z)\}\,\mathrm{d}x + \int_{x=z}^{L} \varepsilon k u'(x; z)\delta u'(x; z)\,\mathrm{d}x = 0 \tag{18}$$

and the sensitivity problem is

$$\begin{aligned}
\delta_u \bar{\Phi} &= k u'(z; z)\delta u'(z; z) - f\delta u(z; z) + \int_{x=0}^{z} \{k\bar{u}'(x; z)\delta u'(x; z) + k u'(x; z)\delta \bar{u}'(x; z) - f\delta \bar{u}(x; z)\}\,\mathrm{d}x \\
&\quad - \varepsilon k u'(z; z)\delta u'(z; z) + \int_{x=z}^{L} \{\varepsilon k\bar{u}'(x; z)\delta u'(x; z) + \varepsilon k u'(x; z)\delta \bar{u}'(x; z)\}\,\mathrm{d}x \\
&= \left[k u'(z; z)\delta u'(z; z) - f\delta u(z; z) - \varepsilon k u'(z; z)\delta u'(z; z) + \int_{x=0}^{z} k\bar{u}'(x; z)\delta u'(x; z)\,\mathrm{d}x \right. \\
&\quad \left. + \int_{x=z}^{L} \varepsilon k\bar{u}'(x; z)\delta u'(x; z)\,\mathrm{d}x \right] + \left[\int_{x=0}^{z} \{k u'(x; z)\delta \bar{u}'(x; z) - f\delta \bar{u}(x; z)\}\,\mathrm{d}x \right. \\
&\quad \left. + \int_{x=z}^{L} \varepsilon k u'(x; z)\delta \bar{u}'(x; z)\,\mathrm{d}x \right] = 0
\end{aligned} \tag{19}$$

Since the kinematic constraint in Eq. (14) is imposed at a non-design boundary, the corresponding constraint for the sensitivity problem is easily obtained as

$$\bar{u}(0; z) = 0 \tag{20}$$

From Eqs. (14) and (20), we can see that δu in Eq. (18) and $\delta \bar{u}$ in Eq. (19) are in the same kinematically admissible space, so the terms in the second bracket in Eq. (19) vanish. The final form of the sensitivity equation and its kinematic constraint are

$$\begin{aligned}
&k u'(z; z)\delta u'(z; z) - f\delta u(z; z) - \varepsilon k u'(z; z)\delta u'(z; z) + \int_{x=0}^{z} k\bar{u}'(x; z)\delta u'(x; z)\,\mathrm{d}x \\
&\int_{x=z}^{L} \varepsilon k\bar{u}'(x; z)\delta u'(x; z)\,\mathrm{d}x = 0
\end{aligned} \tag{21}$$

$$\bar{u}(0; z) = 0 \tag{22}$$

Note that the first three terms in Eq. (21) arise only at the design boundary and act as force terms in the equation. Also, the stiffness terms in Eq. (21) are exactly the same as those of the reference problem

in Eq. (18). For numerical implementation, the same basis functions for the approximation of $\bar{u}$ as those of u are used; therefore, the stiffness matrix from Eq. (18) can be reused as the stiffness matrix for Eq. (21). We will explain more issues of the numerical formulation using two-dimensional problems because the one-dimensional problem with the fictitious domain is not so meaningful.

If kinematic constraint is imposed at the design boundary, more attentions are required to be paid. Instead of the condition in Eq. (12c), consider the fixed design boundary, i.e.,

$$u = 0 \quad \text{at } x = z \tag{23}$$

Taylor's expansion is used again for the perturbed boundary:

$$u(z + \Delta z; z + \Delta z) = u(z; z) + u'(z; z)\Delta z + \bar{u}(z; z)\Delta z + \cdots \tag{24}$$

As the design boundary is also fixed in the perturbed problem, Eq. (24) results in

$$\bar{u}(z; z) = -u'(z; z) \tag{25}$$

In the above, the kinematic constraint for the design boundary in the sensitivity equation is given as the spatial derivative of the solution. Thus, u and $\bar{u}$ have different kinematic constraints. Moreover, the terms in the second bracket in Eq. (19) do not vanish because $\delta\bar{u}$ cannot be zero at the constrained design boundary:

$$\delta\bar{u}(z; z) = -\delta u'(z; z) = -\left.\frac{\mathrm{d}(\delta u)}{\mathrm{d}x}\right|_{x=z} \neq 0 \tag{26}$$

Since u in Eq. (19) is in equilibrium, every point of the domain has zero contribution from those terms in the second bracket except the fixed design boundary. In other words, the nonzero contribution of the terms arises at the fixed design boundary where δu is zero and $\delta\bar{u}$ is not zero, and the value of the contribution can be determined considering the reaction force at the point and Eq. (25). Hansen et al. (2001) mentioned that the nonzero component can be considered as the sensitivity of the incremental work required to move the solution at the reference boundary constraint to its perturbed position.

3.2. Two-dimensional problems

3.2.1. Poisson equation

A two-dimensional heat conduction problem is considered. The domain of interest and its embracing fictitious domain are illustrated in Fig. 1. The differential equation and boundary conditions of the problem are

$$-\nabla \cdot (k\nabla u) = f \quad \text{in } \omega \tag{26a}$$

and

$$u = 0 \quad \text{on } \Gamma_\omega^g \tag{26b}$$

$$(k\nabla u) \cdot \mathbf{n} = 0 \quad \text{on } \Gamma_\omega^h \tag{26c}$$

where $\mathbf{n}$ is the unit vector outward normal to the boundary.

The total potential energy of the whole domain is expressed as

$$\Phi = \int\int_\omega \left\{\frac{1}{2}k\nabla u.\nabla u - fu\right\}\mathrm{d}\omega + \int\int_{\Omega\setminus\omega} \frac{1}{2}\varepsilon k\nabla u \cdot \nabla u\,\mathrm{d}\omega \tag{27}$$

The solution of the problem is obtained from the variational form of the above:

$$\delta_u\Phi = \int\int_\omega \{k\nabla u.\nabla\delta u - f\delta u\}\,\mathrm{d}\omega + \int\int_{\Omega\setminus\omega} \varepsilon k\nabla u \cdot \nabla\delta u\,\mathrm{d}\omega = 0 \tag{28}$$

with

$$u = 0 \quad \text{on } \Gamma_\omega^g \tag{29}$$

Using Eq. (17b) and the formula in Eq. (4), the sensitivity equation for a certain design parameter is derived as

$$\begin{aligned}\delta_u \bar{\Phi} = &\left[\int\int_\omega k\nabla\bar{u}\cdot\nabla\delta u\,\mathrm{d}\omega + \int\int_{\Omega\setminus\omega} \varepsilon k\nabla\bar{u}\cdot\nabla\delta u\,\mathrm{d}\omega\right] \\ &+ \left[\int\int_\omega \{k\nabla u\cdot\nabla\delta\bar{u} - f\delta\bar{u}\}\,\mathrm{d}\omega + \int\int_{\Omega\setminus\omega} \varepsilon k\nabla u\cdot\nabla\delta\bar{u}\,\mathrm{d}\omega\right] \\ &+ \int_{{}^{\mathrm{D}}\Gamma_\omega} \{k\nabla u\cdot\nabla\delta\bar{u} - f\delta\bar{u}\}\mathbf{V}\cdot\mathbf{n}\,\mathrm{d}\Gamma - \int_{{}^{\mathrm{D}}\Gamma_\omega} \{\varepsilon k\nabla u\cdot\nabla\delta\bar{u}\}\mathbf{V}\cdot\mathbf{n}\,\mathrm{d}\Gamma = 0\end{aligned} \tag{30}$$

where the negative sign of the last term is due to the opposite direction of the normal vector when ${}^{\mathrm{D}}\Gamma_\omega$ is viewed from $\Omega\setminus\omega$.

If the kinematic constraint is not imposed on the design boundary, i.e., ${}^{\mathrm{D}}\Gamma_\omega \cap \Gamma_\omega^g = \phi$, the constraint for Eq. (30) is simply

$$\bar{u} = 0 \quad \text{on } \Gamma_\omega^g \tag{31}$$

and the terms in the second bracket in Eq. (30) will vanish as in the one-dimensional case.

If ${}^{\mathrm{D}}\Gamma_\omega \cap \Gamma_\omega^g \neq \phi$, then the kinematic constraint for the perturbed problem is expanded as

$$u(\mathbf{x} + \mathbf{V}\Delta z; z + \Delta z) = u(\mathbf{x}; z) + \nabla u(\mathbf{x}; z)\cdot\mathbf{V}\Delta z + \bar{u}(\mathbf{x}; z)\Delta z + \cdots \tag{32}$$

so ignoring higher order terms leads to

$$\bar{u}(\mathbf{x}; z) = -\nabla u(\mathbf{x}; z)\cdot\mathbf{V} \quad \text{for } \mathbf{x} \in {}^{\mathrm{D}}\Gamma_\omega \cap \Gamma_\omega^g \tag{33}$$

In Eq. (33), we assume the kinematic constraints for the reference and the perturbed problem are identical. Thus, the kinematic constraint for the sensitivity equation can be represented as the gradient of the solution in the design velocity direction. The imposition of (33) is, however, difficult for the fixed-grid analysis since the design boundary does not pass though the grid points. Generally, the problems with fixed design boundaries are not easy to handle in a fixed-grid analysis.

Now we consider the numerical formulation of Eq. (30) using the single-scale fixed-grid method. The terms in the first bracket in the equation form the stiffness matrix of the sensitivity equation, which is the same as that of the reference problem. The terms in the second bracket vanish if the design boundary is not fixed, so we consider the formulation of the last boundary integration terms.

In Fig. 5, an element on a design boundary is illustrated. We parameterize the boundary with a Bezier or a B-spline curve and the vertical movement of the control point of the curve is selected as a design parameter. For the numerical analysis, however, the boundary curve is approximated as a straight line. Nonlinear approximations of the curve for the numerical analysis would considerably improve the solution accuracy, but the consistent use of the nonlinear interpolation of the field variables will make the analysis quite involved. In this work, we choose to use the bilinear interpolation functions for the field variables, but an efficient multiscale adaptive method with dense nodal distributions near the boundary curve will be employed instead. The adaptive scheme will be explained in Section 5.

We approximate the solution on the element shown in Fig. 5 as

$$u^{\mathrm{e}} = \sum_{i=1}^{4} N_i(\xi,\eta) U_i^{\mathrm{e}} \tag{34}$$

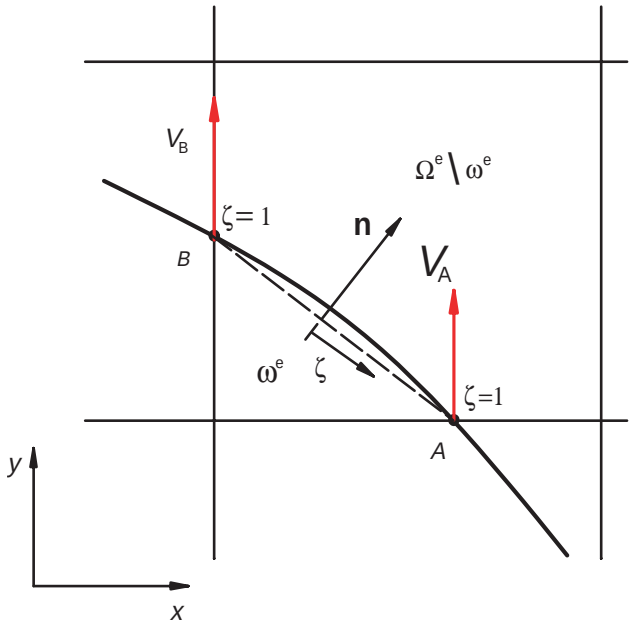

Fig. 5. An element on a design boundary and its boundary velocities at intersection points for the vertical movement of the control point.

where N_i is the bilinear shape function. The element force vector for the sensitivity equation from the last two terms of Eq. (30) is

$$\tilde{\mathbf{f}}^e = -(\mathbf{U}^e)^T \int_{D\Gamma^e_{\omega_A}} \left\{ k\frac{\partial \mathbf{N}^T}{\partial x}\frac{\partial \mathbf{N}}{\partial x} + k\frac{\partial \mathbf{N}^T}{\partial y}\frac{\partial \mathbf{N}}{\partial y} - f\mathbf{N}^T \right\} \mathbf{V}^T\mathbf{n}\, d\Gamma + (\mathbf{U}^e)^T \int_{D\Gamma^e_{\omega_A}} \varepsilon k \left\{ \frac{\partial \mathbf{N}^T}{\partial x}\frac{\partial \mathbf{N}}{\partial x} + \frac{\partial \mathbf{N}^T}{\partial y}\frac{\partial \mathbf{N}}{\partial y} \right\} \mathbf{V}^T\mathbf{n}\, d\Gamma \tag{35}$$

where $\mathbf{U}^e$ and $\mathbf{N}$ are the vector representations of U_i^e and N_i and the design boundary on the element, ${}^D\Gamma^e_\omega$, is approximated as the oblique line, ${}^D\Gamma^e_{\omega_A}$, which is illustrated by the dashed line in Fig. 5. The boundary design velocity $\mathbf{V}$ is also linearly approximated and the normal vector $\mathbf{n}$ is constant on the approximated boundary. For the element in Fig. 5, Eq. (35) is rewritten as

$$\tilde{\mathbf{f}}^e = -(\mathbf{U}^e)^T \int_{-1}^{1} \left\{ k\frac{\partial \mathbf{N}^T}{\partial x}\frac{\partial \mathbf{N}}{\partial x} + k\frac{\partial \mathbf{N}^T}{\partial y}\frac{\partial \mathbf{N}}{\partial y} - f\mathbf{N}^T \right\} \mathbf{V}^T\mathbf{n}\tilde{J}\, d\zeta + (\mathbf{U}^e)^T \int_{-1}^{1} \varepsilon k \left\{ \frac{\partial \mathbf{N}^T}{\partial x}\frac{\partial \mathbf{N}}{\partial x} + \frac{\partial \mathbf{N}^T}{\partial y}\frac{\partial \mathbf{N}}{\partial y} \right\} \mathbf{V}^T\mathbf{n}\tilde{J}\, d\zeta \tag{36}$$

with

$$\mathbf{V} = \left[0, \frac{1-\zeta}{2} V_b + \frac{1+\zeta}{2} V_a \right] \tag{37}$$

The Jacobian $\tilde{J}$ in Eq. (36) relates the coordinate on ${}^{\mathrm{D}}\Gamma^{\mathrm{e}}_{\omega_A}$ and its normalized coordinate ζ, which is the half length of ${}^{\mathrm{D}}\Gamma^{\mathrm{e}}_{\omega_A}$. We mention that the boundary design velocity at intersection points, V_a and V_b in Eq. (37), can be obtained with the parametric location of those points on the boundary. Simple examples will be given in Section 4 (see Chang and Choi, 1992 and Choi and Chang, 1994 for more details).

3.2.2. Plane elasticity problem

From the formulation results of the Poisson problem, the extension of the formulations to plane elasticity problems is straightforward. The total potential energy and the kinematic constraint of a plane structure is

$$\Phi = \int\int_{\omega} \left\{ \frac{1}{2}\mathbf{e}^{\mathrm{T}}\mathbf{C}\mathbf{e} - \mathbf{f}^{\mathrm{T}}\mathbf{u} \right\} \mathrm{d}\omega + \int\int_{\Omega\setminus\omega} \varepsilon \frac{1}{2}\mathbf{e}^{\mathrm{T}}\mathbf{C}\mathbf{e}\,\mathrm{d}\omega \tag{38}$$

with

$$\mathbf{u} = \mathbf{0} \quad \text{on } \Gamma^{g}_{\omega} \tag{39}$$

where $\mathbf{e}$ is the strain vector, $\mathbf{f}$ is the force vector, and $\mathbf{u}$ is the displacement vector.

The first variation of Eq. (38) is given as

$$\delta\Phi = \int\int_{\omega} \{\delta\mathbf{e}^{\mathrm{T}}\mathbf{C}\mathbf{e} - \mathbf{f}^{\mathrm{T}}\delta\mathbf{u}\}\,\mathrm{d}\omega + \int\int_{\Omega\setminus\omega} \varepsilon\delta\mathbf{e}^{\mathrm{T}}\mathbf{C}\mathbf{e}\,\mathrm{d}\omega \tag{40}$$

and the solution sensitivity is obtained from

$$\begin{aligned}\delta\bar{\Phi} = {} & \left[\int\int_{\omega} \delta\mathbf{e}^{\mathrm{T}}\mathbf{C}\bar{\mathbf{e}}\,\mathrm{d}\omega + \int\int_{\Omega\setminus\omega} \varepsilon\delta\mathbf{e}^{\mathrm{T}}\mathbf{C}\bar{\mathbf{e}}\,\mathrm{d}\omega \right] \\ & + \left[\int\int_{\omega} \{\delta\bar{\mathbf{e}}^{\mathrm{T}}\mathbf{C}\mathbf{e} - \mathbf{f}^{\mathrm{T}}\delta\bar{\mathbf{u}}\}\,\mathrm{d}\omega + \int\int_{\Omega\setminus\omega} \varepsilon\delta\bar{\mathbf{e}}^{\mathrm{T}}\mathbf{C}\mathbf{e}\,\mathrm{d}\omega \right] + \int_{{}^{\mathrm{D}}\Gamma_{\omega}} \{\delta\mathbf{e}^{\mathrm{T}}\mathbf{C}\mathbf{e} - \mathbf{f}^{\mathrm{T}}\delta\mathbf{u}\}\mathbf{V}^{\mathrm{T}}\mathbf{n}\,\mathrm{d}\Gamma \\ & - \int_{{}^{\mathrm{D}}\Gamma_{\omega}} \{\varepsilon\delta\mathbf{e}^{\mathrm{T}}\mathbf{C}\mathbf{e}\}\mathbf{V}^{\mathrm{T}}\mathbf{n}\,\mathrm{d}\Gamma \\ = {} & 0 \end{aligned} \tag{41}$$

The kinematic constraint for Eq. (41) is

$$\bar{\mathbf{u}} = 0 \quad \text{on } \Gamma^{g}_{\omega} \tag{42}$$

under the condition of ${}^{\mathrm{D}}\Gamma_{\omega} \cap \Gamma^{g}_{\omega} = \phi$, so the terms in the second bracket in Eq. (41) also vanish.

The last two terms in Eq. (41) form the force vector of the sensitivity equation after numerical formulation. The element force vector for a boundary element is given as

$$\tilde{\underline{\mathbf{f}}}^{\mathrm{e}} = -(\underline{\mathbf{U}}^{\mathrm{e}})^{\mathrm{T}} \int_{-1}^{1} \{\mathbf{B}^{\mathrm{T}}\mathbf{C}\mathbf{B} - \underline{\mathbf{N}}^{\mathrm{T}}\mathbf{f}\}\mathbf{V}^{\mathrm{T}}\mathbf{n}\tilde{J}\,\mathrm{d}\zeta + (\underline{\mathbf{U}}^{\mathrm{e}})^{\mathrm{T}} \int_{-1}^{1} \varepsilon\{\mathbf{B}^{\mathrm{T}}\mathbf{C}\mathbf{B}\}\mathbf{V}^{\mathrm{T}}\mathbf{n}\tilde{J}\,\mathrm{d}\zeta \tag{43}$$

where $\underline{\mathbf{U}}^{\mathrm{e}}$ is the nodal displacement vector of the element and $\underline{\mathbf{N}}$ is the matrix with bilinear shape functions.

4. Numerical examples

In most shape optimization problems, local performance measures such as heat fluxes or the Von Mises stresses, rather than solution itself, are considered as design constraints. Although we use the fixed-grid analysis method and calculate a solution on the fixed grids, the points where the local performances are

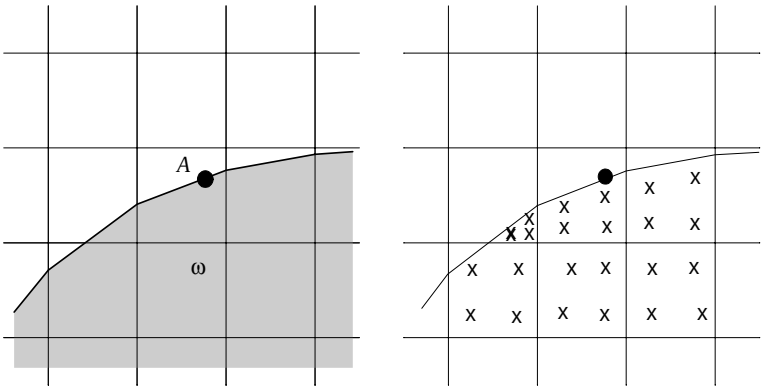

Fig. 6. The neighboring elements used to calculate the local performance on the boundary point A and the Gauss points considered in the least square approximation (×: Gauss points).

evaluated move as the design changes. So, if the local performance is denoted as $\psi(\mathbf{x};z)$, the coordinate $\mathbf{x}$ in $\psi(\mathbf{x};z)$ is not stationary. Therefore, the sensitivity of $\psi(\mathbf{x};z)$ is

$$\frac{\mathrm{d}\psi(\mathbf{x};z)}{\mathrm{d}z}=\frac{\partial\psi}{\partial z}+\sum_{i=1}^{N}\frac{\partial\psi}{\partial x_i}\frac{\partial x_i}{\partial z}=\bar{\psi}+(\nabla\cdot\psi)\cdot\mathbf{V} \tag{44}$$

To calculate Eq. (44), we need the solution for ψ, the solution sensitivity for $\bar{\psi}$, and the boundary design velocity $\mathbf{V}$ at the point of interest.

During the shape optimization process, a domain boundary may move across the element boundary of the fixed grids. In this case, the local performance measure ψ may not be differentiable. Thus, the stress at a point of interest can undergo an abrupt change as the point moves from one element to another element. To avoid the resulting numerical difficulty and obtain the stable estimate of ψ at a given point, ψ is approximated by using ψ's at the stiffness integration points (or the Gauss points) of the neighboring elements. For the approximation, the least square approximation technique is used. Fig. 6 shows the neighboring elements and their Gauss points that are used to calculate the local performance at the desired point. However, the elements lying totally outside the domain of interest are excluded.

4.1. Case study 1: Heat flux sensitivity

Fig. 7(a) illustrates a structure with a unit thermal conductivity, whose top edge is under uniform heat flux $q=1$. The bottom edge of the structure has zero temperature and both side edges are insulated. For the fixed-grid analysis with oblique boundary approximation, a fictitious domain with 5×5 fixed mesh in Fig. 7(b) is introduced.

The design boundary is the right edge of the structure and is parameterized using a Bezier curve with three control points:

$$\mathbf{p}(u)=\sum_{i=0}^{2}B_{i,2}(u)\mathbf{Q}_i\quad(0\leqslant u\leqslant 1) \tag{45}$$

with

$$B_{i,k}(u)=\binom{k}{i}u^i(1-u)^{k-i} \tag{46}$$

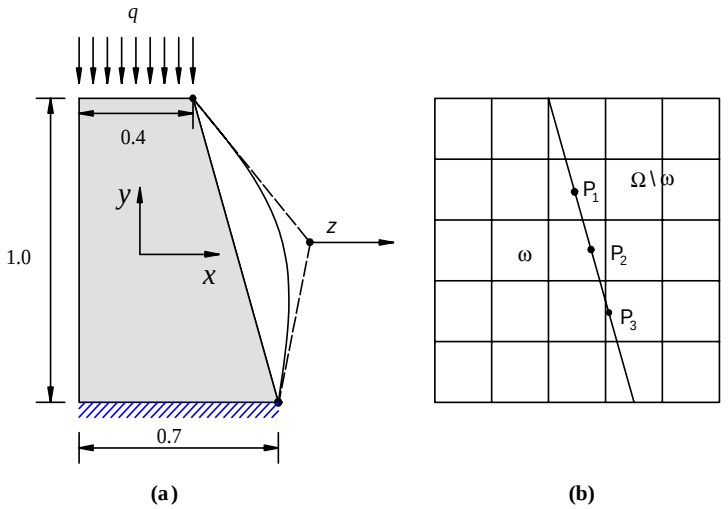

Fig. 7. A heat conduction problem: (a) the domain of interest and (b) its fixed mesh with the fictitious domain.

The initial positions of the control points are $\mathbf{Q}_0 = [0.7, 0]$, $\mathbf{Q}_1 = [0.55, 0.5]$ and $\mathbf{Q}_2 = [0.4, 1]$ and the x-directional movement of $\mathbf{Q}_1$ is selected as the design parameter z.

Using Eq. (45), the boundary design velocity is evaluated as

$$\mathbf{V}(u) = \frac{\mathrm{d}}{\mathrm{d}z}\mathbf{p}(u) = B_{1,2}(u)[1, 0] = [2u(1-u), 0] \tag{47}$$

by which the velocities at intersection points and points of performance measure can be calculated with their parametric locations.

In Table 1, we list the design sensitivity results at three boundary points whose parametric locations are $u = 0.3$, 0.5 and 0.7, respectively. The numerical values in the parentheses denote the heat flux components in the horizontal and vertical directions. Since the semi-analytic sensitivity is available, it will be interesting to check the effect of the perturbation Δz on the accuracy of the sensitivity by the finite difference scheme. For the finite difference sensitivity evaluation, the following forward difference scheme is used:

$$\frac{\mathrm{d}\psi}{\mathrm{d}z} \approx \frac{\psi(z + \Delta z) - \psi(z)}{\Delta z}$$

In Table 1, the sensitivities by the finite difference method for various values of Δz are compared with the semi-analytic sensitivities. Unless Δz is very small, the sensitivity calculation by the finite difference method may not be accurate. Moreover, the system stiffness matrix should be constructed and factorized as many

Table 1
Sensitivity results of heat flux and comparison with the finite difference results

	Semi-analytic (present) method	Finite difference method		
		$\Delta z = 10^{-2}$	$\Delta z = 10^{-3}$	$\Delta z = 10^{-4}$
P_1	(2.05e−1, 1.21e0)	(2.00e−1, 1.20e0)	(2.04e−1, 1.21e0)	(2.05e−1, 1.21e0)
P_2	(−2.52e−1, 9.99e−1)	(−2.49e−1, 9.96e−1)	(−2.51e−1, 9.99e−1)	(−2.52e−1, 9.99e−1)
P_3	(7.77e−1, 3.80e−1)	(5.86e−1, 4.25e−1)	(7.57e−1, 3.85e−1)	(7.75e−1, 3.80e−1)

times as design parameters are perturbed in the finite difference method. On the other hand, only the force terms in Eq. (36) or Eq. (43)need to be changed in the proposed semi-analytic method so that the stiffness matrix is constructed and factorized once regardless of the number of design parameters.

4.2. Case study 2: Elasticity problem with simple clamped beam

A structure with the same geometry as in the previous example is considered. Fig. 8 shows that the bottom edge of the structure is fixed and a horizontal force $F = 1.0 \times 10^5$ is imposed on the upper right corner. The material has a Young's modulus $E = 2.0 \times 10^8$ and Poisson's ratio $v = 0.3$. The fixed mesh in Fig. 7(b) is also used for this problem. The design sensitivities of the Von Mises stresses at the points of interest are listed in Table 2. Again, a small value of Δz should be used to get accurate results for the finite difference method.

4.3. Case study 3: Gripper example

Fig. 9 shows the upper half geometry of a compliant gripper whose mechanism is based on the elastic deformation of the structure. The geometry of the gripper is composed of eight B-spline curves which approximate the boundaries of the result from topology optimization (Jang et al., 2003).

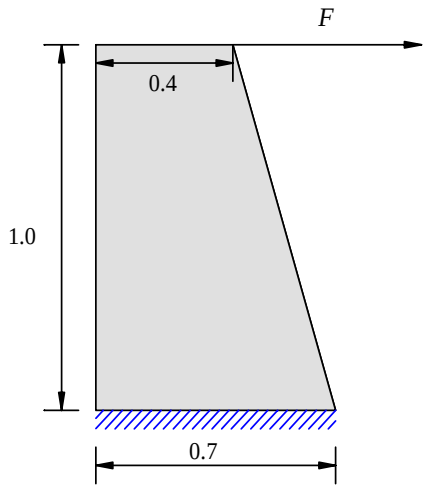

Fig. 8. A cantilever example.

Table 2
Sensitivity results of the Von Mises stress and comparison with the finite difference results

	Semi-analytic (present) method	Finite difference method		
		$\Delta z = 10^{-2}$	$\Delta z = 10^{-3}$	$\Delta z = 10^{-4}$
P_1	−1.13e6	−1.13e6	−1.13e6	−1.13e6
P_2	−1.99e6	−1.97e6	−1.99e6	−1.99e6
P_3	−0.89e6	−1.06e6	−0.90e6	−0.89e6

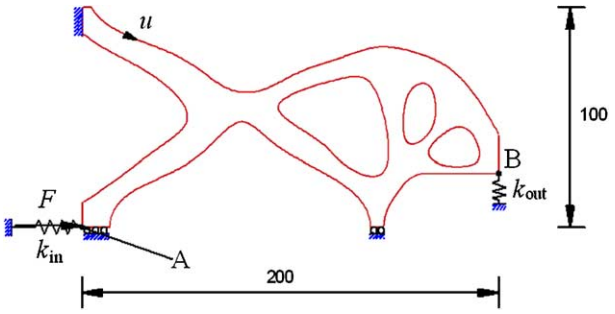

Fig. 9. A compliant gripper.

Table 3
Sensitivity results of the Von Mises stress for the gripper example

	u	Semi-analytic (present) method	Finite difference method ($\Delta z = 10^{-5}$)
P_1	0.187	2.54e1	2.53e1
P_2	0.253	2.37e1	2.35e1
P_3	0.383	−1.27e2	−1.27e2
P_4	0.463	8.17e1	8.17e1
P_5	0.517	4.73e1	4.72e1

In Fig. 9, the input force $F = 5.0 \times 10^4$ is imposed at point A and a spring with $k_{in} = 2.0 \times 10^4$ is also attached at the point to characterize the actuator, such as a piezo-electric actuator. At the output point B, another spring with $k_{out} = 2.0 \times 10^3$ is attached to control the stiffness of the gripper. The material properties of the gripper are $E = 2.0 \times 10^5$ and $v = 0.3$. The upper most boundary of the gripper is parameterized with the 3rd order B-spline curve with 12 control points. The vertical movement of the 6th control point is considered as the design parameter. The sensitivities of the Von Mises stresses at 12 points on the design boundary are calculated and listed in Table 3, which shows the good agreement of the calculated sensitivities with the converged results of the finite difference method.

Note that, while the original boundaries of the gripper are B-spline curves, the approximated boundaries for analysis are composed of piecewise linear segments. So the discrepancy between original and approximated boundaries may deteriorate the analysis accuracy. The accuracy may be improved by using higher-order boundary approximations. For example, one may consider piecewise quadratic approximations of the boundary and its velocity field by using three points, i.e., point A, point B and the middle point between A and B (see Fig. 5). In that case, the approximation order of a solution should be consistent with the approximation order of the boundaries. In this work, this quadratic approximation was not pursued. Instead, the boundary curve is discretized with many piecewise straight lines by using dense fixed mesh. The resulting numerical cost is reduced by the adaptive scheme implemented within the wavelet-Galerkin method which will be explained in the next section.

5. Sensitivity analysis for multiscale wavelet-Galerkin method

The fixed-grid analysis using the oblique boundary curve approximation can achieve much faster shape optimization in cooperation with the adaptive analysis by the multiscale wavelet-Galerkin method (Jang et al., 2004). In this section, we discuss the sensitivity analysis for the multiscale solution of the multiscale wavelet-Galerkin method.

Consider that the domain Ω in Fig. 1 is divided into $2^{J_x} \times 2^{J_y}$ elements ($J_x = J_y = J$ for ease of explanation). Then, the approximated solution with the resolution level J is expressed as

$$u_J = \sum_{k,l} s_{J,k,l}\phi_{J,k,l}(x,y) \tag{48a}$$

$$= \sum_{k,l} s_{j_0,k,l}\phi_{j_0,k,l}(x,y) + \sum_{j=j_0}^{J-1}\sum_{m=1}^{3}\sum_{k,l} d^m_{j,k,l}\psi^m_{j,k,l}(x,y) \tag{48b}$$

where $\phi_{j,k,l}$ is the bilinear shape function (or the hat interpolation scaling function) whose sub index j represents the support size (or resolution) of the function, and k and l are translation indices. Also, $\psi^m_{j,k,l}$ in Eq. (48b) is the hat interpolation wavelet whose super index indicates the difference in the measuring direction of the function (see Jang et al., 2004 for more details). Eq. (48a) is the single-scale representation of the approximated solution, and Eq. (48b) is the multiscale representation of the solution. The hat interpolation wavelets $\phi_{j,k,l}$ and $\psi^m_{j,k,l}$ are similar to the hierarchical bases discussed in, e.g., Yserentant (1986). However, the hierarchical bases are element-level multiscale bases and require isoparametric mapping to handle domains with general boundaries.

A transformation matrix $\mathbf{T}^{\text{Total}}_J$ converts the multiscale solution into the single-scale solution: (the procedure to construct $\mathbf{T}^{\text{Total}}_J$ is given in Jang et al., 2004)

$$\mathbf{U}_J = \mathbf{T}^{\text{Total}}_J \mathbf{W}_J \tag{49}$$

where $\mathbf{U}_J$ is the vector composed of the single-scale solution $s_{j,k,l}$ and $\mathbf{W}_J$ is the multiscale solution vector with $s_{j_0,k,l}$ and $d^m_{j,k,l}$.

The multiscale system equation for a reference problem is derived from the multiscale transformation of the single-scale system equation: (see Jang et al., 2004)

$$\widehat{\mathbf{K}}_J \mathbf{W}_J = \hat{\mathbf{F}}_J \tag{50}$$

with

$$\widehat{\mathbf{K}}_J = (\mathbf{T}^{\text{Total}}_J)^{\text{T}} \mathbf{K}_J \mathbf{T}^{\text{Total}}_J \tag{51}$$

$$\widehat{\mathbf{F}}_J = (\mathbf{T}^{\text{Total}}_J)^{\text{T}} \mathbf{F}_J \tag{52}$$

where $\mathbf{K}_J$ is the stiffness matrix for the single-scale system equation and can be obtained using equations in Section 2. Also, F_J is the force vector for the single-scale system equation.

Using the difference-checking nature of wavelets as an error indicator of the adaptive analysis, the multiscale system equation in (50) is progressively solved from low to high resolutions. In Fig. 10, a flowchart for the multiscale adaptive analysis is illustrated. For the adaptive scheme, two thresholding parameters ($\delta^u > \delta^l > 0$) are employed. Assume that the analysis at the resolution level $j+1$ with wavelets of $\{\phi_{j_0,k,l}, \{\psi^m_{j',k,l}\}_{j'=j_0,\ldots,j}\}$ is finished and the wavelet coefficients $\{d^m_{j',k,l}\}_{j'=j_0,\ldots,j}$ are calculated. Then the following procedure is used for the adaptive analysis at the next resolution level $j+2$: (see Jang et al., 2004 for more details)

- Exclude the wavelet $\psi^m_{j,k,l}$ from the basis set if its coefficient $|d^m_{j,k,l}| < \delta^l_j$.
- Preserve $\psi^m_{j,k,l}$ in the basis set if $\delta^l_j \leqslant |d^m_{j,k,l}| < \delta^u_j$.
- Add child wavelets of $\psi^m_{j,k,l}$ into the basis set if $|d^m_{j,k,l}| \geqslant \delta^u_j$.

The discrete sensitivity equation for the single-scale solution can be written as

$$\mathbf{K}_J \bar{\mathbf{U}}_J = \widetilde{\mathbf{F}}_J \tag{53}$$

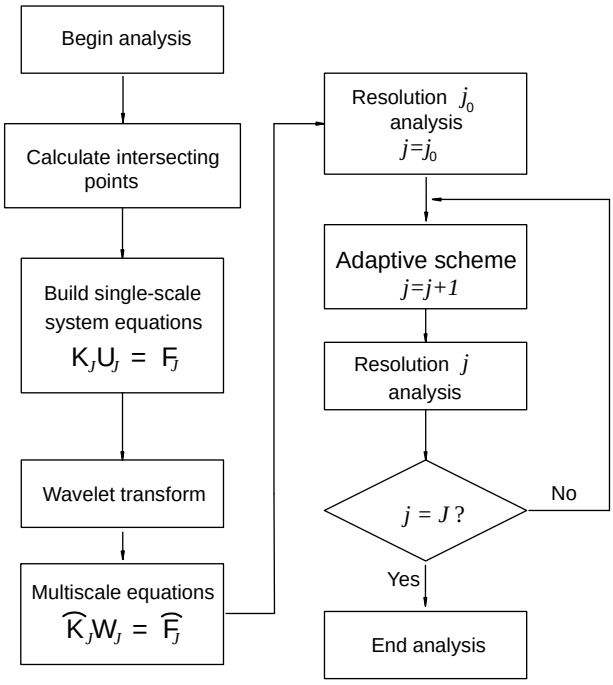

Fig. 10. Multiscale adaptive analysis.

The stiffness matrix in Eq. (53), as we discussed in Section 3, is the same as that of the reference problem, and the force vector can be obtained using Eqs. (36) or (43). The transformation equation in Eq. (49) can be also applied to find the solution sensitivity

$$\bar{\mathbf{U}}_J = \mathbf{T}_J^{\text{Total}} \bar{\mathbf{W}}_J \tag{54}$$

so the multiscale solution sensitivity equation is derived as

$$\widehat{\mathbf{K}}_J \bar{\mathbf{W}}_J = \widehat{\widetilde{\mathbf{F}}}_J \tag{55}$$

with

$$\widehat{\widetilde{\mathbf{F}}}_J = (\mathbf{T}_J^{\text{Total}})^{\mathrm{T}} \widetilde{\mathbf{F}}_J \tag{56}$$

The adaptive scheme, which is used for solving the reference problem of Eq. (50), is also applied for the sensitivity problem of Eq. (55). Thus, faster shape sensitivity analysis is expected by the multiscale wavelet-Galerkin method.

6. Conclusions

The analytic shape sensitivity for the fixed-grid method using the boundary approximation by piecewise oblique lines was derived. The shape sensitivity analyses for two-dimensional Poisson problems and plane elasticity problems were explicitly carried out. In the proposed fixed-grid method, the force terms in the sensitivity equations appeared only at the boundary elements. Thus, the calculation of the force terms required the boundary velocity field on the boundary elements, and the field was approximated linearly in

terms of the velocities at the intersection points of the original boundary curve and the edges of the fixed finite elements. The analytic sensitivity derived in this investigation was validated by the comparison with the numerical sensitivity. We also showed that the analytic sensitivity was applicable for the multiscale wavelet-Galerkin method and presented the procedure to implement the shape sensitivity within the multiscale method. When the multiscale fixed-grid method is extended to three-dimensional problems, the proposed method is expected to greatly speed up the whole shape optimization process.

Acknowledgments

Prof. K.K. Choi at the University of Iowa offered a great opportunity for the first author to learn his theory on sensitivity analysis during the first author's stay at the Center for Computer-Aided Design at the University of Iowa. The authors thank the comments of the reviewers without which some points would have remained unclear.

References

Bennett, J.A., Botkin, M.E., 1985. Structural shape optimization with geometric description and adaptive mesh refinement. AIAA J. 23 (3), 458–464.

Chang, K.H., Choi, K.K., 1992. A geometry-based parameterization method for shape design of elastic solids. Mech. Struct. Mach. 20 (2), 215–252.

Choi, K.K., Chang, K.H., 1994. A study of design velocity field computation for shape optimal design. Finite Elements Anal. Des. 15, 317–341.

Choi, K.K., Kim, N.H., in press. Design sensitivity analysis of linear and nonlinear structural system.

Garcia, M.J., Steven, G.P., 1998. Fixed grid finite elements in elasticity problems. Engng. Comput. 16 (2), 154–164.

Hansen, J.S., Liu, Z.S., Olhoff, N., 2001. Shape sensitivity analysis using a fixed basis function finite element approach. Struct. Multidisc. Optim. 21, 177–195.

Haug, E.J., Choi, K.K., Komkov, V., 1986. Design Sensitivity Analysis of Structural Systems. Academic Press Inc.

Jang, G.W., Kim, Y.Y., Choi, K.K., 2002. Shape optimization using the wavelet-Galerkin method. The Second China–Japan–Korea Joint Symposium on Optimization of Structural and Mechanical Systems 2002, Busan, Korea, pp. 865–870.

Jang, G.W., Kim, Y.Y., Choi, K.K., 2003. Remesh-free shape optimization using the wavelet-Galerkin method and its applications to MEMS actuator design. WCSMO-5 Lido de Jesolo 2003, pp. 121–122.

Jang, G.W., Kim, J.E., Kim, Y.Y., 2004. Multiscale Galerkin method using interpolation wavelets for two-dimensional elliptic problems in general domains. Int. J. Numer. Meth. Engng. 59, 225–253.

Kim, N.H., Chang, Y., 2003. Eulerian shape optimization with fixed grid. 44th AIAA/ASME/ASCE/AHS/ASC Structures, Structural Dynamics, and Materials Conference 2003, Norfolk, Virginia.

Kim, N.H., Chang, Y., submitted for publication. Eulerian shape design sensitivity analysis and optimization with fixed grid. Comput. Methods Appl. Mech. Engrg.

Yao, T.M., Choi, K.K., 1989. 3-D shape optimal design and automatic finite element regridding. Int. J. Numer. Meth. Engng. 28, 369–384.

Yserentant, H., 1986. On the multilevel splitting of finite element spaces. Numer. Math. 49, 379–412.